Airframe Scattering of Engine Fan Noise

Yueping Guo[1] and Russell H. Thomas[2]
NASA Langley Research Center

This paper presents a study on aircraft engine fan noise scattering by the airframe structure, using a methodology in the framework of geometric acoustics with extensions to account for features that are important for aircraft noise but are absent in classic geometric acoustics. Methods to parameterize engine fan noise sources for scattering calculation are presented and the important feature of source coherence is discussed, with examples given to demonstrate its effects in experimental data and in computation. The scattering results calculated for the Boeing 787 aircraft are presented and analyzed, for both the inlet and the aft fan component, and for both the broadband and the tonal noise. Many features are shown to be consistent with, and/or provide explanations for, observations in flight test data. The methodology and capabilities described in this study are written into the NASA PAASc code and represent a necessary and significant improvement in the accuracy and capabilities for acoustic scattering prediction while meeting the rigorous requirements of aircraft system noise assessments and design studies.

Nomenclature

B_n = base function of source distribution
C = cost function
C_{nk} = scattering coefficient for n^{th} source and k^{th} path
c_0 = mean sound speed
D = noise directivity
E_m = error function
F_n = auxiliary function
G = Green's function
k_0 = acoustic wavenumber
K_n = number of rays for the n^{th} source
N_s = number of source elements
p = acoustic pressure
Q = source power spectral density
Q_n = discretized source power spectral density
q = source strength
r = propagation path length
R_{nk} = propagation path length in flow for n^{th} source and k^{th} path
t = time
$\mathbf{x}$ = microphone location coordinate
$\mathbf{y}$ = source location coordinate
δ = Dirac delta function
ψ_{nk} = scattering coefficient for the n^{th} source and k^{th} ray
Π = noise spectrum
Π_m = measured noise spectrum
Ω = angular frequency
τ = time delay

[1] Senior Research Engineer, Aeroacoustics Branch, AIAA Associate Fellow, Seal Beach, CA 90740, USA.
[2] Senior Research Engineer, Aeroacoustics Branch, AIAA Associate Fellow, Hampton, VA 23681, USA.

I. Introduction

The scattering of aircraft engine fan noise by the airframe is a significant contributing effect to total aircraft noise, affecting the noise certification levels at required measurement locations and the community noise levels around airports (Refs [1]-[11]). The impacts may be in the form of increases in noise amplitudes and changes in noise directivity. The scattering mechanisms responsible for these effects include reflections by the fuselage and the wings, sharp-edge diffractions by the trailing edges of the wing and the high-lift elements, and smooth-surface diffractions by the fuselage and the leading edges of the wings. The total scattering effects also depend on the features of the noise source; in this case, fan source noise (Refs [12]-[18]). The important features, for scattering, can include their locations, amplitude variations, spectra, coherence properties, and directivity patterns.

In this paper, these fan noise scattering effects are quantified by calculations, using the Boeing 787 aircraft geometry at realistic flight conditions, for both the inlet and the aft fan noise and for both the incoherent broadband noise and the coherent tonal noise. The objectives are to discuss the process of the computational methodology, the source specification, and to demonstrate the features in the scattering results and the underlying physical mechanisms responsible. In practical applications, the scattering effects, either computed or measured, can be used in total aircraft noise prediction where the engine noise is typically predicted or measured for isolated engines without the airframe. In this case, the scattering effects are added to the noise of the isolated engines to yield the total engine noise at flight conditions (Refs [19], [20]). Conversely, the scattering effects can also be used for component separation where flight test data are decomposed into various noise components with the scattering effects extracted out of the flight noise data (Refs [21], [22]).

While the scattering of aircraft engine noise by the airframe has always been recognized as necessary, its quantification by numerical computation has not been straightforward or practical, certainly for aircraft system noise assessments. Many methods have been developed within the aeroacoustics community and applied over many years. The challenge is developing a method that achieves sufficient accuracy and provides necessary capabilities, while remaining feasible within the the computational turnaround times required of aircraft system noise and design. Readily available, easily implemented methods have been limited in physics and capabilities or unrealistic for the requirements of a full aircraft computation. In fact, for NASA aircraft system noise assessments, Propulsion Airframe Aeroacoustic (PAA) interaction experiments have been relied on to make data-based predictions for the PAA interaction effects for both flow and acoustic scattering interaction types, including for fan noise scattering (Refs [1], [5]-[9], [19], [20]). Even with many configurations and noise source types in an experimental database, this data-based prediction approach was never seen as the optimum. The efficient computation of PAA acoustic scattering by a physics based, direct method applied to to the specific source characteristics and geometry of interest has always been the desired goal for application to NASA's Aircraft System Noise (ASN) capabilities.

One challenge to compute fan noise scattering is the availability of computational methods that can be applied accurately and efficiently to realistic aircraft configurations at realistic flight conditions. Mathematically, the computation of sound scattering involves the solutions of the governing equations of sound waves with prescribed source definitions, subject to boundary conditions on the scattering bodies in the acoustic medium. There are various methods to achieve this. The suitability of these methods for the application of aircraft noise scattering, however, is determined not solely mathematically. Instead, it is dictated by practical constraints and requirements, such as the desired prediction accuracy, the available computational resources, the required turn-around time, and the realistic noise source characteristics. To meet the most critical requirements and to balance various aspects of aircraft noise applications, the computational methodology is developed under the framework of geometric acoustics (Refs [23]-[27]), for its numerical efficiency, its formulations that closely mimic the physics of wave propagation, and its straightforward and logical implementation of realistic noise source features.

The methodology, however, differs and extends the classical geometric acoustics in various features and capabilities that are important to aircraft noise but are absent in classic geometric acoustics. These include the effects of mean flow, noncanonical geometry, and surface impedance in the formulations of sound reflection and diffraction. Since the unique approach of geometric acoustics is to model and formulate each individual physical mechanism, the formulations for the reflection and diffraction have been extended to account for all the features important to aircraft noise (Refs [28], [29]). The extended new formulations have been systematically validated by both canonical problems and realistic aircraft applications (Refs [30], [31]), including for the NASA/Boeing PAA & ASN Flight Test (Refs [10], [11]) with a Boeing 787 aircraft, which is used in this paper to demonstrate the scattering features. To accomplish the goal of efficient computation of acoustic scattering, this new methodology and formulation has been developed into the Propulsion Airframe Aeroacoustic Scattering (PAASc) Code. Note that the same formulation is used for a limited version where the reflection capability is intentionally turned off, the PAA Shielding Attenuation, PAAShA Code (Ref [30]).

Another challenge in computing the scattering of engine noise by the aircraft is the source specifications. In engine noise studies, attention has traditionally been more on the far field noise than on the source specifications. To understand the physical mechanisms of engine fan noise sources, much has been achieved in the past few decades (Refs [12]-[18], [32]). However, quantitative definitions of the sources are still not readily available for engineering applications of scattering computations, which require the specifications of source features such as source location, source strength distribution, spectrum, and directivity. Because the far field noise of isolated engines has been extensively measured and studied in the past, and can be relatively easily obtained in future studies, a process of source parameterization is used in this paper to derive the source features from the far field noise. The process involves the mathematical method of least squares data fitting, the physical constraint of non-negative source amplitude, and the empirical determination of the source locations, shapes, and dimensions, for the individual noise components. The process is clearly empirical and is clearly not unique. It is found to be sufficient for engine fan noise scattering computation because the inlet fan and aft fan noise can be regarded as being radiated respectively from the inlet lip cross-section and the fan duct exit plane, the former as a circular distribution and the latter as an annular distribution. The other source quantities such as amplitude variation and directivity are then derived by the method of least squares to fit the far field noise that can be obtained by measurements, numerical simulations, or empirical predictions.

One of the advantages of geometric acoustics is that the sound propagation and scattering follows individual paths, or rays, and the amplitudes and the phases of the sound waves along the paths are all computed. This makes it natural and easy to implement and compute the effects of source coherence, which is an important feature of engine fan noise with its tonal components highly coherent and its broadband components highly incoherent. The source coherence does not affect the linear acoustic quantities such as the acoustic pressure. However, the interferences, or the lack of them, between waves from different noise components and/or between waves from different propagation paths, can significantly affect the quadratic quantities such as the sound spectrum and the acoustic energy, which are quantities almost exclusively used as noise metrics. The significant effects of interferences due to source coherence in sound scattering will be illustrated with comparisons to test data (Refs [33]-[34]), and the effects on engine fan noise scattering will be discussed.

For inlet fan broadband noise, the scattering will be shown to be small, about 0.5 dB at measurement locations where there is scattering. This is expected, because the inlet noise sources are upstream of the wing so that the scattering in the forward quadrant is entirely due to the fuselage that is not an efficient reflector because of its curved surface. In the aft quadrant where there is scattering from the wing, the inlet noise itself has very low amplitude, making the scattering effects less relevant. The scattering of aft fan broadband noise is more significant than the inlet noise, with the wings and the high-lift systems providing more efficient reflecting surfaces. The general features of aft fan broadband noise scattering are the reflection to the forward quadrant by the local geometry of the wings, the reflection to the lateral locations by the surfaces between the engines, and the large scattering amplitude up to about 7 dB, resulting from the combined effects of curved surface reflection and the source directivity, which redirects the sound waves of high-amplitudes in aft angles to forward angles of low-amplitude incident waves.

The broadband noise scattering is additive on an energy basis because the noise sources are highly incoherent so that the reflection and diffraction simply add acoustic energy. The tonal noise, however, is generated by highly coherent sources so that the direct, reflected and diffracted waves strongly interfere with each other, leading to scattering patterns that can result in either a noise increase or noise decrease. The coherent interference is also present between the inlet and the aft fan components, and between engines. The scattering mechanisms for broadband noise still hold for tonal noise, such as the strong scattering of aft fan noise to forward angles and to lateral locations, which is consistent with flight test data (Refs [10], [11], [31]). In addition, the coherent interferences of tonal noise result in high amplitude peaks and dips in the scattered pattern. The noise increase in this case can be as high as 12 dB for one engine and 15 dB for two engines at discrete measurement locations. The high amplitude scattering is the cumulative effect of reflection, source directivity, coherent addition of acoustic pressure, and the potential interference dip of the noise from the isolated engines.

Accurate and efficient calculations of fan noise scattering for real aircraft is essential to provide higher fidelity, more accurate results for aircraft system noise predictions. The analysis and understanding of the scattering mechanisms can also illuminate other aspects. An example will be presented, where the different peak radiation angles of aft fan noise, between isolated and installed engines, will be explained by the flight effects of forward scattering, Doppler amplification, and fan duct flow refraction. The combination of the three can move the peak radiation angle upstream by as much as 40 to 50 degrees, consistent with observations in flight test data.

The scattering calculations will also be used to assess the accuracy and applicability of other approximate and empirical approaches that have been readily available previously. For example, the NASA Aircraft Noise Prediction Program (ANOPP) has a module, WING, that has been widely used. The formulation in WING implements reflection from planar surfaces only and shielding is based on an implementation of the Fresnel diffraction theory for a semi-

infinite barrier (Refs [35], [36]). Therefore, while computationally efficient for system noise calculations, the WING module calculates the scattering effect in a very rudimentary way, in both the methodology and the geometry, and its handling of scattering for multiple engines and/or multiple components is greatly over-simplified, missing important scattering features, especially for tonal noise. These will be discussed regarding scattering physics and the error in using a method like that in WING will be quantified by numerical examples.

II. Source Parameterization

For the computation of noise scattering, the noise sources need to be specified, which, for aircraft engine fan noise, is a very challenging task because the understanding of such sources is by no means complete and sufficient, despite decades of research and significant advancements. In fact, for practical fan noise measurement and prediction, most efforts have been focused on the far field noise, bypassing the issue of source definition. Thus, the source definition for scattering computations cannot be expected to be specified precisely and uniquely. Instead, the source characterization is likely to make use of the far field noise, either from direct measurement or from empirical prediction, to empirically derive source properties that are most relevant to the scattering computation. The goal of scattering calculation is to predict the increase or decrease of the noise levels due to scattering. Thus, it is not required to have a complete definition of the sources for scattering calculation. For example, source quantities such as absolute magnitudes and spectral shapes are not relevant. This makes it feasible to use a parameterization process to extract the relevant source properties, which is the process followed in this paper.

The process begins with empirically determining the source locations, distribution shapes, and distribution dimensions, with the source amplitudes or source power spectral densities within the source distribution as unknowns. Then, the unknowns are solved for by using the method of least squares to fit the far field noise with necessary physical constraints on the solutions, such as nonnegative power spectral densities of the sources. Clearly, this process is highly empirical and nonunique, with the scattering computation affected by the empirical assumptions of the source locations and source shapes. Thus, it is important to make these assumptions to represent the physics as close as possible. For example, it is logical to specify the source region for inlet noise as the circular cross-section of the inlet nacelle at the inlet lip location, and similarly, for aft fan noise, as the annular cross-section of the aft fan duct at the exit plane, which are respectively illustrated in Fig. 1.

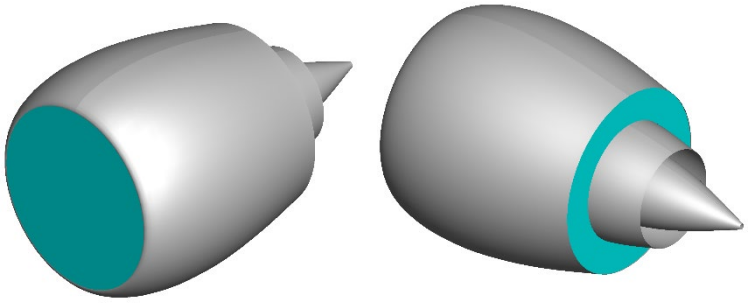

Fig. 1 Illustration of fan noise source region for inlet (left) and aft fan (right) noise.

The formulation of the least squares method starts with the acoustic pressure at the microphone location $\mathbf{x}$, denoted by $p(\mathbf{x})$,

$$p(\mathbf{x}) = \int_{\mathbf{y}} q(\mathbf{y}) G(\mathbf{x},\mathbf{y}) D(\mathbf{x},\mathbf{y}) d^3\mathbf{y} \tag{1}$$

where $q(\mathbf{y})$ is the unknown source amplitude at the source location $\mathbf{y}$, $G(\mathbf{x},\mathbf{y})$ is the Green's function, and $D(\mathbf{x},\mathbf{y})$ is the noise directivity. The objective of the method can be chosen to be the solutions for the source amplitude $q(\mathbf{y})$, likely the case if the sources are coherent. For incoherent sources, it is more convenient to select the source power spectral density as the unknown. To this end, the noise power spectral density can be constructed by multiplying the acoustic pressure by the complex conjugate of itself and taking ensemble average, leading to

$$\Pi = \left\langle p(\mathbf{x}) p^*(\mathbf{x}) \right\rangle = \int_{\mathbf{y}} \int_{\mathbf{y}'} \left\langle q(\mathbf{y}) q^*(\mathbf{y}') \right\rangle G(\mathbf{x},\mathbf{y}) D(\mathbf{x},\mathbf{y}) G^*(\mathbf{x},\mathbf{y}') D(\mathbf{x},\mathbf{y}') d^3\mathbf{y} d^3\mathbf{y}' \tag{2}$$

where the noise power spectral density is denoted by Π, the ensemble average is represented by the brackets which only include the source amplitudes in the integrand function because the other quantities are all deterministic, and the complex conjugate is indicated by the asterisk. For incoherent sources, the ensemble average of the source amplitudes is simply given by

$$\left\langle q(\mathbf{y})q^*(\mathbf{y}')\right\rangle = Q(\mathbf{y})\delta(\mathbf{y}-\mathbf{y}') \tag{3}$$

with $Q(\mathbf{y})$ being the source power spectral density and δ being the Dirac delta function. By substituting this into the result (2), the delta function can be used to eliminate one of the two volume integrals so that the noise power spectral density becomes

$$\Pi = \int_{\mathbf{y}} Q(\mathbf{y})\left|G(\mathbf{x},\mathbf{y})D(\mathbf{x},\mathbf{y})\right|^2 d^3\mathbf{y} \tag{4}$$

where $Q(\mathbf{y})$ is the unknown quantity. This quantity is in general a continuous function of the source coordinates $\mathbf{y}$. It can be expressed either by discretizing the physical source region into small volumes or by representing the source distribution by modes of known shapes. In both representations, the source power spectral density can be written as

$$Q(\mathbf{y}) = \sum_{n=1}^{N_s} Q_n B_n(\mathbf{y}) \tag{5}$$

where N_s is the number of source elements, equal to either the number of discretized physical sources or the number of modes, B_n is the base function of the source element and Q_n is its unknown amplitude. With this, the source power spectral density can be rewritten as

$$\Pi(Q_n) = \sum_{n=1}^{N_s} Q_n F_n(\mathbf{x}) \tag{6}$$

with the dependence of the noise power spectral density Π on the unknown amplitude of the source elements explicitly indicated on the left side of the result and the function F_n given by

$$F_n(\mathbf{x}) = \int_{\mathbf{y}} B_n(\mathbf{y})\left|G(\mathbf{x},\mathbf{y})D(\mathbf{x},\mathbf{y})\right|^2 d^3\mathbf{y} \tag{7}$$

which only involves known quantities.

The noise power spectral density Π can now be matched with measurements, or independent predictions of the far field noise, and an error function, E_m for the m^{th} microphone or measurement/prediction location, can be defined by the difference between the two, namely,

$$E_m = \Pi(Q_n) - \Pi_m(\mathbf{x}) \tag{8}$$

where Π_m is used to denote the measured or predicted noise power spectral density. From this, a cost function is defined as

$$C = \sum_{m=1}^{N_m} \left|E_m\right|^2 = \sum_{m=1}^{N_m} \left|\Pi(Q_n) - \Pi_m\right|^2 \tag{9}$$

with the summation over all the N_m microphones. The equation for the method of least squares can be derived by setting the derivatives of the cost function, with respect to the unknown quantity, to zero, leading to

$$\frac{\partial C}{\partial Q_i} = \sum_{m=1}^{N_m}\left[\Pi(Q_n) - \Pi_m\right]\frac{\partial \Pi}{\partial Q_i} = 0 \tag{10}$$

for $i = 1, 2, 3, \ldots, N_m$. It is straightforward to substitute the result for the noise power spectral density to derive

$$\sum_{n=1}^{N_s}\left[\sum_{m=1}^{N_m}\left|G(\mathbf{x})\right|^4 F_n(\mathbf{x})F_i(\mathbf{x})\right]Q_n = \sum_{m=1}^{N_m}\Pi_m(\mathbf{x})\left|G(\mathbf{x})\right|^2 F_i(\mathbf{x}) \tag{11}$$

which represent a set of N_m equations for the N_s unknowns.

The solutions to the least squares equation give the source distribution amplitudes. To do this, measurements, or predictions, of the noise power spectral densities at the microphone locations are needed. For example, these can be obtained by empirical predictions implemented in ANOPP, also known as the Krejsa method (Ref [37]) for aircraft engine fan noise. The number of equations is not necessarily equal to the number of unknowns and the equations are likely to be ill-conditioned or close to singular. Thus, special methods are required to solve the equations (e.g., singular value decomposition). Furthermore, the solutions by the method of least squares may only be mathematical with non-physical features. An example is negative values for the power spectral density. In this case, additional physical constraints need to be incorporated in the solution process. This can be done either formally by using Lagrange multiplier in the least squares equations, or heuristically by rescaling the results to meet the physical constraint, which is acceptable for the calculations of noise scattering because the absolute amplitudes of the sources are irrelevant in such calculations.

With this solution process, examples of the source parameterization are shown in Fig. 2, for a representative nacelle (not that of on the Boeing 787). This result is for incoherent broadband noise sources, with the left plot for inlet noise and the right plot for aft fan noise. The computed solutions use far field data generated by the Krejsa method, and are

the source power spectral densities, as a function of frequency and radial distance on the source disc. The radial distance is normalized by the nacelle diameter at the inlet lip for inlet noise so that the range of horizontal axis in the left plot is from zero to 0.5, and by the outer diameter of the aft fan duct at the exit so that the range of the horizontal axis in the right plot is from about 0.22 to 0.5.

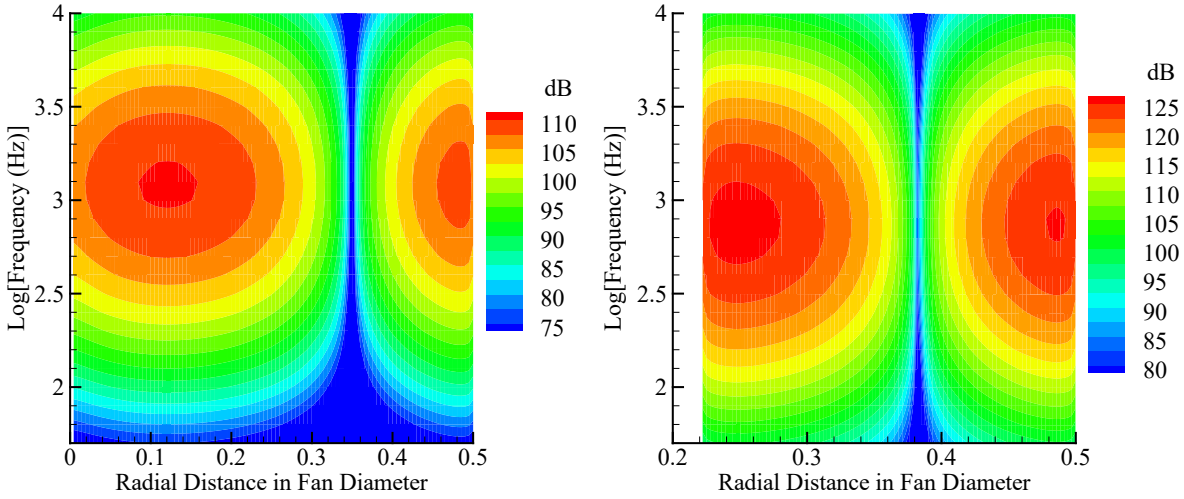

Fig. 2 Incoherent source amplitude for inlet (left) and aft fan (right) noise.

For coherent tonal noise sources, the formulation is different. The main difference is that the unknown quantity in this case is the source amplitude $q(\mathbf{y})$, instead of its power spectral density. The derivation of the equations and the solution processes, however, follow similar steps. Thus, the mathematics will not be repeated here. Fig. 3 shows the calculated source amplitudes, at the blade passage frequency (BPF) and its two harmonics, as a function of the radial distance in the source disc, for inlet tones in the left plot and aft fan tones in the right plot. Again, since scattering calculations are not concerned with the absolute noise levels, it is the shapes of the source distribution that are important.

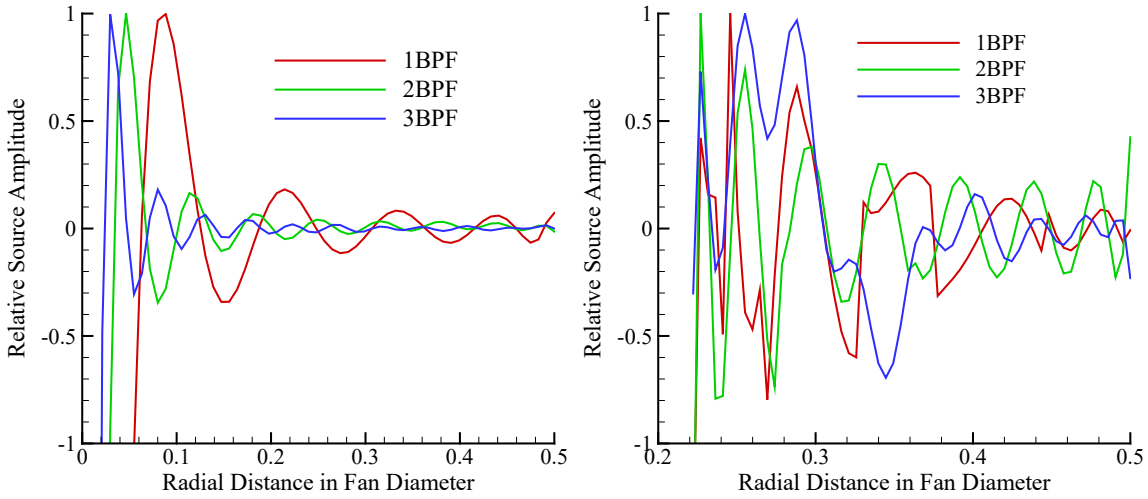

Fig. 3 Coherent tonal source amplitudes for inlet (left) and aft fan (right) noise.

III. Effect of Source Coherence

Aircraft engine fan noise consists of both coherent tonal noise and incoherent broadband noise. The two have very different characteristics. This is mainly because noise metrics such as sound pressure level (SPL) and sound intensity are quadratic quantities. Thus, when there are multiple components in the linear quantity of sound pressure, either due to multiple sources or due to multiple propagation paths, there is interaction, or lack of it, between the components in the construction of the quadratic noise metrics. This can be clearly demonstrated by a simple example where sound waves are radiated by a source, which take two propagation paths to reach the microphone, as illustrated in Fig. 4,

where one path is directly from the source to the microphone with path length r_1 and the other is the path with a reflection by a surface with the total path length r_2.

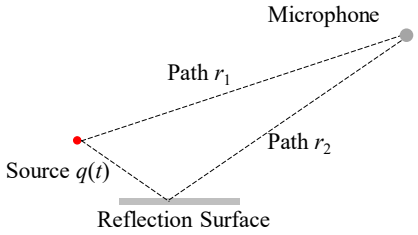

Fig. 4 Illustration of multiple path propagation.

For this simple example, the linear acoustic pressure, $p(t)$ as a function time t, consists of two components, namely,

$$p(t) = \frac{1}{r_1} q(t - r_1 / c_0) + \frac{1}{r_2} q(t - r_2 / c_0) \tag{12}$$

where c_0 is the sound speed and q is the source amplitude that has an autocorrelation, denoted by $Q(\tau)$ as a function of the time delay τ, given by the standard definition,

$$Q(\tau) = \left\langle q(t) q(t+\tau) \right\rangle \tag{13}$$

which defines the coherence properties of the source. The quadratic quantity of the ensemble average of the squared pressure, which is related to other sound metrics, can be easily derived as

$$\left\langle p^2(t) \right\rangle = \frac{1}{r_1^2} Q(0) + \frac{1}{r_2^2} Q(0) + \frac{2}{r_1 r_2} Q\left(\frac{r_2 - r_1}{c_0} \right) \tag{14}$$

The first two terms on the right-hand side are the contributions from the two propagation paths independently and the last term is the contribution from the integrations between the two. Clearly, the interaction term depends on the source autocorrelation, with its argument determined by the difference between the two propagation paths, and hence, the coherence feature of the source can significantly affect the noise generated by the source.

This simple example not only clearly illustrate the physics of the source coherence in sound propagation, it also shows the natural and logical way to implement the source coherence in the framework of geometric acoustics where sound propagation, reflection and diffraction are all treated as rays. Thus, for N_s sources with K_n propagation paths for the n^{th} source, the linear acoustic pressure in frequency domain is given by the sum from all sources and all paths, namely,

$$p(\omega) = \sum_{n=1}^{N_s} \sum_{k=1}^{K_n} q_n \frac{C_{nk}}{R_{nk}} e^{\mathrm{i} k_0 \psi_{nk}} \tag{15}$$

where ω is the angular frequency, q_n is the amplitude of the nth source, k_0 is the acoustic wavenumber, and C_{nk}, R_{nk}, and ψ_{nk} are the scattering coefficient, the propagation path length with flow effect, and the phase function, respectively, of the k^{th} path of the n^{th} source. The sound spectrum can be constructed from the acoustic pressure according to the standard definition,

$$\Pi(\omega) = \left\langle p(\omega) p^*(\omega) \right\rangle \tag{16}$$

Which, by simple substitution of the acoustic pressure, leads to

$$\Pi(\omega) = \sum_{n=1}^{N_s} \sum_{k=1}^{K_n} \sum_{n'=1}^{N_s} \sum_{k'=1}^{K_{n'}} \frac{C_{nk} C^*_{n'k'}}{R_{nk} R_{n'k'}} Q\left[k_0 (R_{nk} - R_{n'k'}) \right] e^{\mathrm{i} k_0 (\psi_{nk} - \psi_{n'k'})} \tag{17}$$

The effects of the source coherence are accounted for by the source autocorrelation function when the propagation distances of two paths are not equal. In implementation of this formulation under the framework of geometric acoustics, the propagation distance of each individual path is naturally computed as part of the ray tracing calculation, and the scattering coefficient represents the effects of physical features of direct propagation, reflection, sharp edge diffraction, and smooth surface diffraction (Refs [28], [29]).

To demonstrate the effects of source coherence, two cases are presented here, both of which have test data with one for a coherent source and the other for an incoherent source. The computations are for both coherent and incoherent source so that the comparisons between the two and with the test data clearly reveal the coherence effects. The first case is the test in the Quiet Flow Facility (QFF) at the NASA Langley Research Center, reported in Ref [33]. The test uses a coherent laser spark source, located on one side of a NACA 0012 airfoil, to generate coherent sound waves, and the scattering from the leading and the trailing edge of the airfoil is measured by microphones on the other side

of the airfoil. Because of the coherent nature of the source and the sound waves, there is strong interference between the two components, respectively from the leading and the trailing edge of the airfoil, in both the frequency and spatial domains. The wave patterns on the airfoil surface are shown in Fig. 5, with the coherent source indicated by the black dot at 10 kHz, for both the upper and the lower surface, the latter being flipped upside down for easy visual. The patterns are characterized by the strong interferences with high peaks and sharp dips.

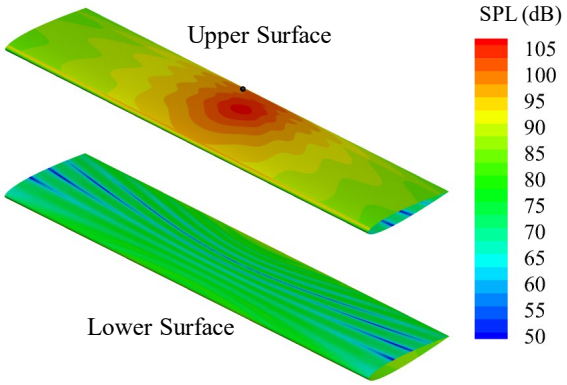

Fig. 5 Wave patterns on NACA 0012 airfoil for a coherent source.

The comparisons for this case are shown in Fig. 6, both between the coherent (red solid curve) and the incoherent (blue dash curve) predictions and with QFF test data (green curve or symbol). The case is for a wind tunnel flow Mach number of 0.16, an airfoil angle of attack of 13 degrees, and a source location on the upper side of the airfoil at 70% of the airfoil chord from its leading edge. The detailed test setup has been reported previously (Refs [30], [33]) and is also illustrated in the figure, with the source indicated by the blue dots and the measurement locations by the black dots. The left plot shows the difference in sound pressure level (ΔSPL), between the installed and the isolated source, as a function of frequency at a fixed spatial location indicated by the black dot below the airfoil, and the right plot shows the integrated ΔSPL in the 7.5 kHz octave band as a function of the flow direction coordinates. The comparison of the coherent prediction with test data shows very good agreement. The incoherent prediction, on the other hand, misses all the interference features in both the frequency and the spatial domain, and thus, contains large errors in comparison with test data.

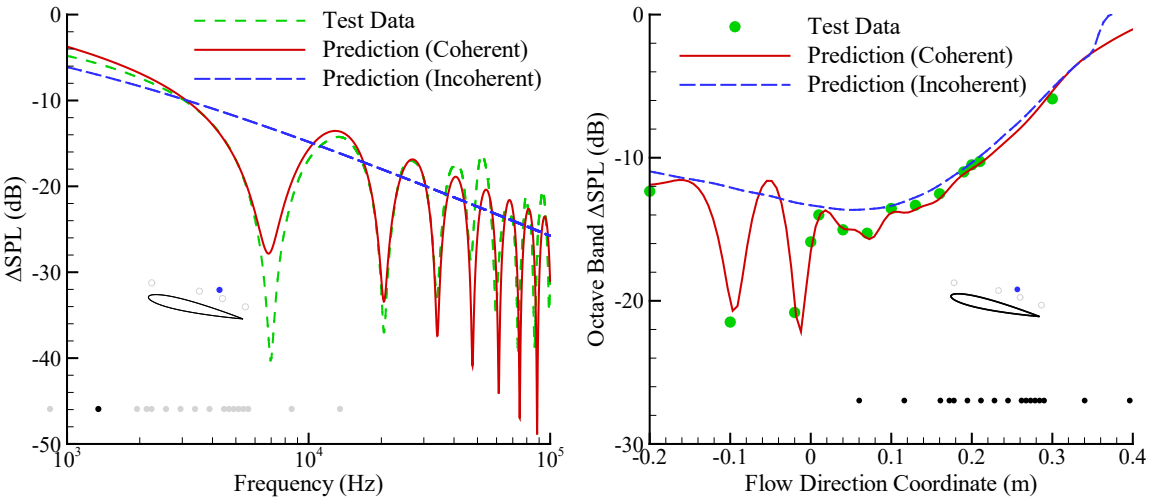

Fig. 6 Comparisons between coherent and incoherent predictions and with QFF test data.

The second case to illustrate the effects of source coherence involves the test in the NASA Langley 14- by 22-Foot Subsonic Tunnel on a 5.8% scale model of the hybrid wing body (HWB) concept, using a broadband noise simulator to generate aft radiating incoherent noise (Ref [34]). The source is located on the upper side of the aircraft model and the measurement locations are below the aircraft so that the shielding effect due to the HWB body is measured. Because the source is incoherent, no interference is expected, and the noise levels essentially follow the rule of

spherical spreading above the aircraft on the side of the source location. This is predicted and shown in Fig. 7 for the noise levels on the upper surface of the HWB model. The patterns are characterized by the smooth variations with decreasing levels from the source location, typical of incoherent sources, even in the presence of scattering.

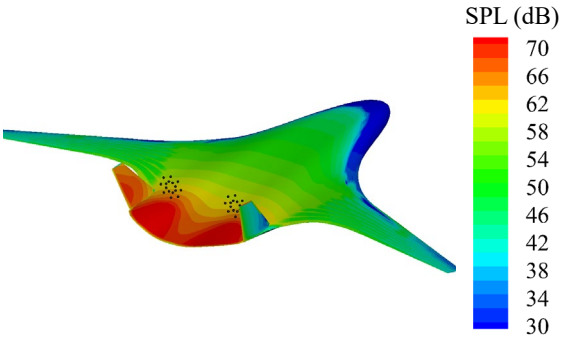

Fig. 7 Incoherent sound pressure levels on HWB.

Below the HWB aircraft, the noise is due to scattering, representing the effects of noise shielding. The comparisons of the shielding effects, defined as the difference in sound pressure levels between the installed and the isolated sources and represented by ΔSPL, are given in Fig. 8 for the 1/3 octave band centered at 10 kHz, with no mean flow and with the aircraft at an angle of attack of 13 degrees. The results are shown as a function of the polar angle in the aircraft symmetry plane below the HWB model. The incoherent prediction is given by the red solid curve, the coherent prediction by the blue dash curve, and the test data by the green dots. Clearly, the incoherent prediction agrees with the test data very well, while the coherent prediction contains large errors due to the interference dips in the polar angle domain.

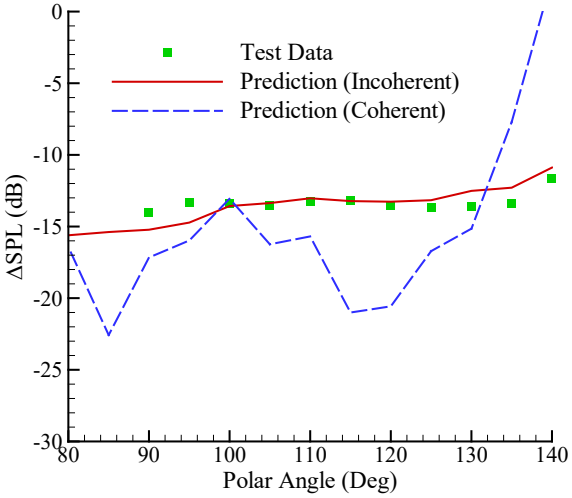

Fig. 8 Comparisons of HWB shielding between coherent and incoherent predictions and with data.

IV. Incoherent Broadband Fan Noise Scattering

The setup for scattering calculations for real aircraft applications is shown in Fig. 9, where the full-scale Boeing 787 aircraft is on the flight path and the calculations are done for microphones on a hemisphere 800 feet away from the aircraft. The Boeing 787 aircraft was used in the flight test summarized in Refs [10] and [11], and an example of validation with the flight test data has been reported in Ref [31]. The computational microphone grid is in the far field below the aircraft, where polar angles range from 10 to 170 degrees, with the 90-degree polar angle being the overhead position and zero being the engine inlet axis, and azimuthal angles from -90 to 90 degrees with zero azimuthal angle being the flyover plane. For calculations corresponding to flight test configurations, the engine on the left of the pilot is at full power and the other is set at idle power. Calculations are done also for two engines at full power with the results discussed in a later section. The scattering effects are presented by the difference in sound pressure levels, between the aircraft and the isolated engine, and are denoted by ΔSPL. Positive values of ΔSPL signify noise increase while negative values indicate noise decrease. The source locations for the inlet and the aft fan component are shown

in Fig. 1 on the cross-section of the nacelle at the inlet lip location and on the cross-section of the fan duct at its exit location, respectively. For broadband noise, the calculations are done first in narrow bands with 64 Hz bandwidth, and the results are then integrated into 1/3 octave bands for output. For tonal noise, which will be discussed in a subsequent section, the calculations are done in single frequencies.

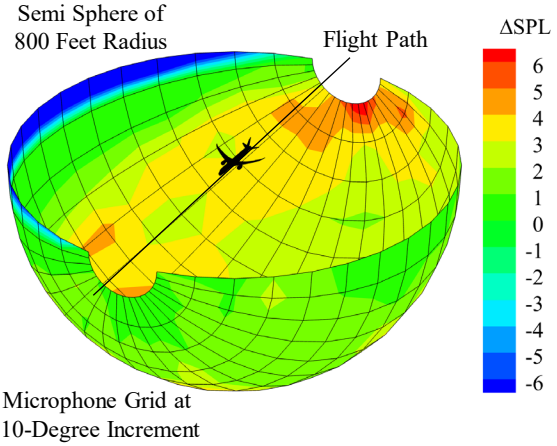

Fig. 9 Setup for scattering calculation for Boeing 787.

Incoherent broadband fan noise of aircraft engines consists of two components, namely, the inlet and the aft fan component. Because of their incoherent nature, there is essentially no interactions between the two and their scattering calculations can be done individually, providing the noise changes due to scattering for each of the two components. The noise for an isolated engine is predicted by the Krejsa method, providing the far field noise levels that are used to derive the source characteristics, by the process described in an earlier section. The source parameterizations, mainly the source location, amplitude, and directivity, are then used in the scattering calculations. The amplitude distributions are shown in Fig. 2. In discretizing the source distribution for calculation, further simplifications are possible. For example, the source amplitude distributions show that for most frequencies, the high amplitude sources are at two radial locations. Thus, the radial discretization can be just two sources at the two high amplitude locations along the radial line. Another example is that at low frequencies, below about 316 Hz for the inlet source and about 100 Hz for the aft fan source, the source amplitude does not vary significantly in the radial direction. In this case, the radial discretization can be simply one source. Physically, this is because at low frequencies, the acoustic wavelength is larger than the cross-section dimension so that the variations are small.

Examples of the scattering effects for incoherent broadband fan noise are shown in Fig. 10 for the inlet noise in the left plot and for the aft fan noise in the right plot, where the contour levels are ΔSPL for the 1/3 octave band of 1000 Hz. The results on the hemisphere are presented in planar view for easier visual inspection. The aircraft flies from left to right, as indicated by the aircraft at the centers of the plots, at a Mach number of 0.28 with a flight profile typical of takeoff operations. For visual comparison, the two plots are on different scales for the contour amplitudes and the maximum contour level is given on each plot.

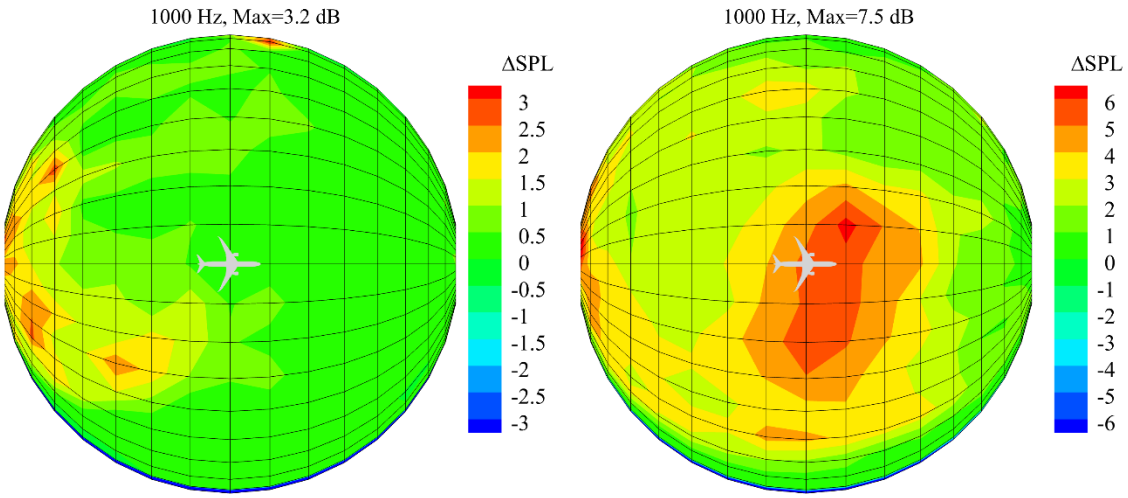

Fig. 10 Scattering of inlet (left) and aft fan (right) broadband noise.

The inlet broadband noise scattering shown in the left plot of Fig. 10 reveals small effects in the forward quadrant where inlet noise is relevant, with a noise increase of about 0.5 dB, mostly due to reflections by the fuselage. The noise sources are located at the inlet lip location, upstream of the wing, so that the effects of the wing are the smooth surface diffraction by the leading edge of slat. However, this diffraction only contributes to locations above the wing, and thus, is not present in the results shown in the left plot of Fig. 10. The fuselage also has smooth surface diffraction for the inlet noise, which is very small due to the heavily attenuated surface waves around the fuselage. There are noise increases of about 2.5 dB at some locations in the aft quadrant in the downstream directions, which are of little practical value because the inlet noise is negligibly small at such locations, even with a few dB increase due to scattering.

The aft fan broadband noise scattering has very different characteristics than the inlet component, as shown by the right plot in Fig. 10, both in the amplitudes of the noise increase and in the scattering pattern. The aft fan noise experiences reflections from the wings as the noise propagates downstream of the fan duct so that the aft quadrant sees a noise increase of about 3 to 5 dB at most aft quadrant locations. The strongest scattering occurs in the region slightly upstream of the overhead location, with a noise increase up to about 7.5 dB, due to the combined effects of reflection from the leading-edge portion of the wing surface and the source directivity. This is illustrated in Fig. 11, where the insert shows that downstream propagating noise from the aft fan source is reflected to upstream locations by the leading-edge portion of the wing surface. This reflection more than doubles the energy levels at the upstream locations because the directivity of the aft noise peaks at aft angles, shown by the blue curve in the figure as a function of the polar angle, and thus, the reflected noise has amplitudes higher than those of the isolated source at forward angles, making the noise increase more than 3 dB, as would be the case from energy doubling.

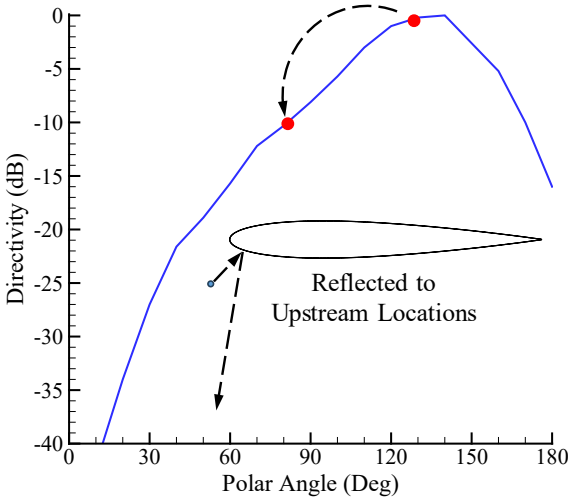

Fig. 11 Illustration of aft fan noise scattering to forward quadrant.

The forward scattering feature helps explain the often observed and sometime puzzling aft fan noise at angles close to or upstream of overhead location in flight tests (Refs [21], [22]). Empirical predictions of aft fan noise for isolated engines, which are usually based on experimental data of static engines without aircraft flight effects, have a directivity that peaks in the aft quadrant around 130 or 140 degrees from the inlet axis. This is in sharp contrast to flight test data, where the peak radiation angle is often observed close to the overhead position of 90 degrees, or even in the forward quadrant. There are potentially many flight effects that may cause the peak radiation angle moving forward. The scattering effect of the wing, discussed above, is one of them, and the others include the flight Doppler amplification and the refraction of the fan duct flow. Fig. 12 shows how these three flight effects may change the aft fan noise directivity from the blue solid curve, representing the polar directivity for isolated engine, which is the same blue curve shown in Fig. 11 predicted by the Kresja model in ANOPP, to the black solid curve for the directivity that includes all three flight effects. The changes due to the individual effects are also illustrated in the figure by the dashed curves. With the three flight effects, the peak radiation angle of aft fan noise shifts close to the overhead direction and the peak becomes very broad, both of which are features observed in flight test data.

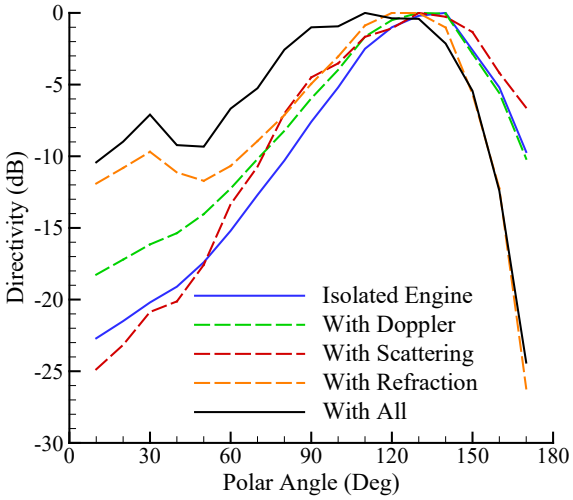

Fig. 12 Changes of aft fan broadband noise directivity due to flight effects.

The scattering patterns shown in Fig. 10 are asymmetrical with respect to the flyover plane because only one engine is at full power. It is also interesting to note the strong scattering to the lateral directions, which occurs more to the idle engine side due to the presence of the pylons and the relatively flat airframe geometry between the engines (i.e., the lower surface of the fuselage and the root portions of the wings). The high levels of scattering to the idle engine side, from light green to brown contour colors in the left plot and from light yellow to red contour colors in the right plot, cover larger spatial ranges than the full power engine side because the reflecting surfaces between the engines are much larger than those on the outer side of the full power engine, resulting in more reflections to the idle engine side. The slanted shapes of the high-level scattering patterns are indications of the elongated reflection area between the engines. This is consistent with flight test data that show higher noise levels at lateral locations than at flyover locations, which is also the case for tonal noise scattering, as will be shown in the next section.

V. Coherent Tonal Fan Noise Scattering

Tonal noise is highly coherent meaning that strong interactions can be expected between multiple source components and/or between multiple propagation and scattering paths. Thus, the scattering calculations for coherent tonal fan noise need to include all components in a simultaneous computation. For the present case, the components are the inlet tones and the aft fan tones, each having its own source location, amplitude, and directivity. With these, the total fan tonal noise scattering is computed, and an example is shown in Fig. 13 for the BPF tone in the left plot. For comparison, the total broadband noise scattering for the 1000 Hz 1/3 octave band is also shown in the right plot of this figure, even though the incoherent broadband noise scattering can be computed and applied separately for each individual component, as discussed in the previous section. For easier visual comparison, the contours in the two plots are on different scales and the maximum levels for each is given in the plots.

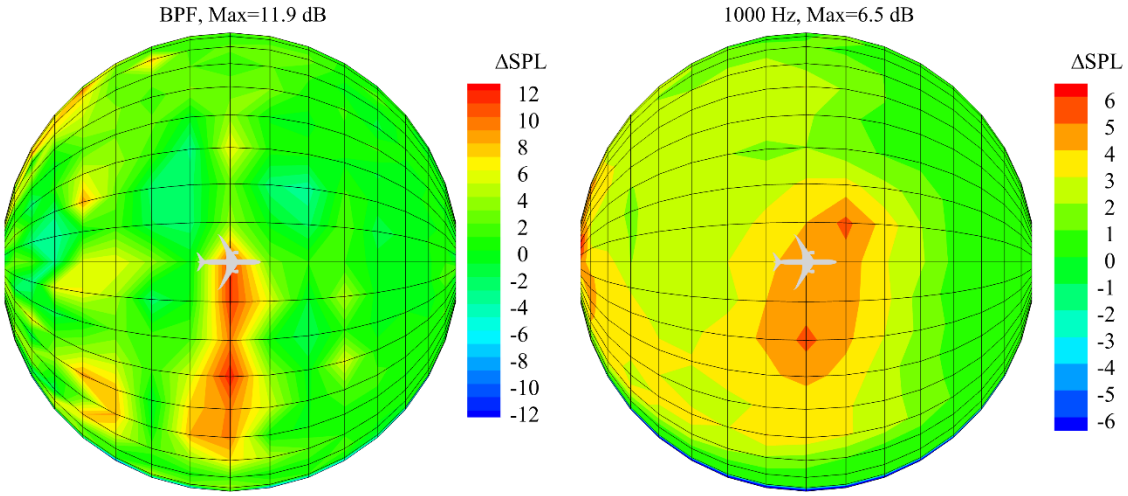

Fig. 13 Scattering of total tonal (left) and total broadband (right) noise.

By comparing the tonal and the broadband noise scattering, it can be seen that there are similar and different features between the two. Similarities include the reflections of the aft fan source to the forward directions, the reflections by the large surfaces between the engines, and the weak scattering of the inlet sources by the fuselage. All these can be clearly seen in the two plots in Fig. 13.

There are many features in the tonal noise scattering which are different from the broadband noise scattering and are due to the coherent interferences. The noise increases due to the tonal noise scattering can be much higher than the broadband noise scattering, up to about 11.9 dB for the former compared to 6.5 dB for the latter. Three factors contribute to the high scattering levels for tonal noise. The first is that coherent reflection means addition of acoustic pressure for the direct propagation and the reflection, while incoherent reflection means energy addition between the two. In the simple case where the direct propagation and the reflection have the same amplitude at the source and the reflection is by a flat rigid surface, the coherent reflection can add 6 dB, while the incoherent reflection can only add 3 dB for this simple reflection. In the application discussed here, the direct and the reflected waves have different amplitudes, due to the directivity of engine fan noise. Thus, more noise can be scattered from high amplitude radiation angles from the source to other microphones, which is the second factor and is the same mechanism for broadband noise scattering, discussed in the previous section and illustrated by Fig. 11. The third factor is the coherent interferences of the noise components for the isolated engine, which may produce low level dips in SPL for the isolated engine at some locations. Since the scattering effects are measured by the difference in SPL between the installed and the isolated sources, low level dips in the latter can amplify the scattering metrics ΔSPL.

Another very noticeable feature of coherent scattering is the high amplitude peaks and sharp dips in the ΔSPL contours. In the left plot of Fig. 13, there are patches of light blue color, corresponding to noise decreases of about 6 dB, which is absent for incoherent scattering that always leads to noise increases wherever there is direct radiation from the engine. This is again due to the pressure addition for the coherent reflection by which the direct and the reflected waves can potentially cancel each other for ΔSPL to reach negative infinity. The sharp dips are limited only by the distributed sources that have slightly different dip locations. The addition of the contributions from all the sources then produces low amplitude areas of finite noise decreases.

VI. Application of Fan Noise Scattering

In practical applications, the calculation of fan noise scattering can be used in total aircraft noise prediction where the engine noise is typically predicted or measured for isolated engines without the airframe. In this case, the scattering effects are added to the noise of the isolated engines to yield the total engine noise at flight conditions (Refs [19], [20]). Conversely, the scattering effects can also be used for component separation where flight test data are decomposed into various noise components with the scattering effects extracted out of the flight noise data (Refs [21], [22]). In this section, a few aspects of the application are discussed, in relation to the prediction of aircraft system noise, by ANOPP, for example.

Most commercial aircraft have two engines, and some have four. The case of one engine is discussed in the previous two sections only to reveal and understand the scattering mechanisms and to be consistent with the flight tests summarized in Refs [10] and [11]. It is natural to ask if the results for one engine, or one full power and one idle

engine, can be used to account for multiple engines. For dual-engine applications, the total noise is sometimes predicted for one engine and 3 dB is then added to account for the second engine. The results of the previous two sections clearly show that this is not a correct approach, because the scattering effects are not symmetrical in azimuthal angles, as shown by Fig. 13, where the strong scattering occurs in the lateral angles on the idle engine side for both the broadband and the tonal component. The idea of simply doubling the results only works if both the noise of the isolated engine and the scattering effects are symmetrical in azimuthal angles.

Considering the symmetry of the aircraft geometry, the engine installation, and the microphone locations, it is tempting to use the results for one engine, flip the results with respect to the symmetry plane and add the results to account for the second engine, which may seem to be better than the approach of doubling the one-engine results. While this works for the incoherent broadband noise, since no interactions are expected between the two engines, it is not the correct approach for the coherent tonal noise, because there are additional interferences between the two engines. The flip-and-add approach assumes the two engines are incoherent, and thus, follow energy addition; however, coherent tonal noise involves pressure addition. To illustrate, Fig. 14 shows the scattering of coherent total BPF noise for two engines at the same power where the direct calculation with the two engines is shown in the left plot and the results from the flip-and-add approach are shown in the right plot. The symmetrical patterns in the figure are expected. The scattering effects, however, are significantly different between the two. The correct direct calculation shown in the left plot contains higher peaks with sharper shapes in the contour maps than the incorrect approach shown in the right plot. The differences are due to the additional interferences between the two engines, correctly captured by the direct calculation but absent in the add-and-flip approach.

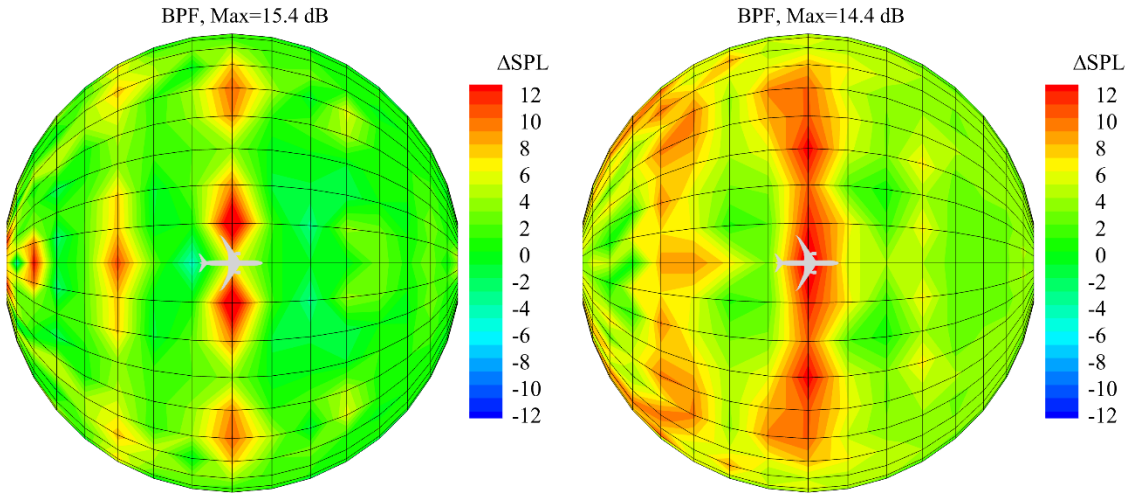

Fig. 14 Scattering of tonal noise for two engines from direct calculation (left) and flip-and-add (right).

In addition to how two engines are accounted for in the prediction, another issue that directly affects the application of the scattering effects concerns whether the effects, namely ΔSPL, can be applied on individual components before the components are summed to derive the total noise. Again, the incoherent broadband noise can be treated using the flip-and-add approach, as discussed in previous sections. For coherent components, however, it has been emphasized that the scattering effects need to be accounted for simultaneously, with all components included. The application of ΔSPL needs to be on the total tonal noise for the isolated engine, not individual components. To further emphasize the importance of correctly dealing with coherent scattering, two approaches are used to compute the scattered total tonal noise, both of which start with the same predictions for the isolated engines. One approach, the correct one, is to sum the two tonal components for the isolated engines, namely, the inlet and the aft fan tones. The total tonal noise for the isolated engines is then used to calculate the total scattering effects. The two are added together to predict the total tonal noise in flight. The second approach, the incorrect one, is to account for the scattering effects individually for the inlet and the aft fan component. Thus, the prediction for the isolated engines, the calculation of the scattering, and the addition of the effects of scattering are all done separately for each component, and the total tonal noise is derived at the last step by adding the components at flight conditions.

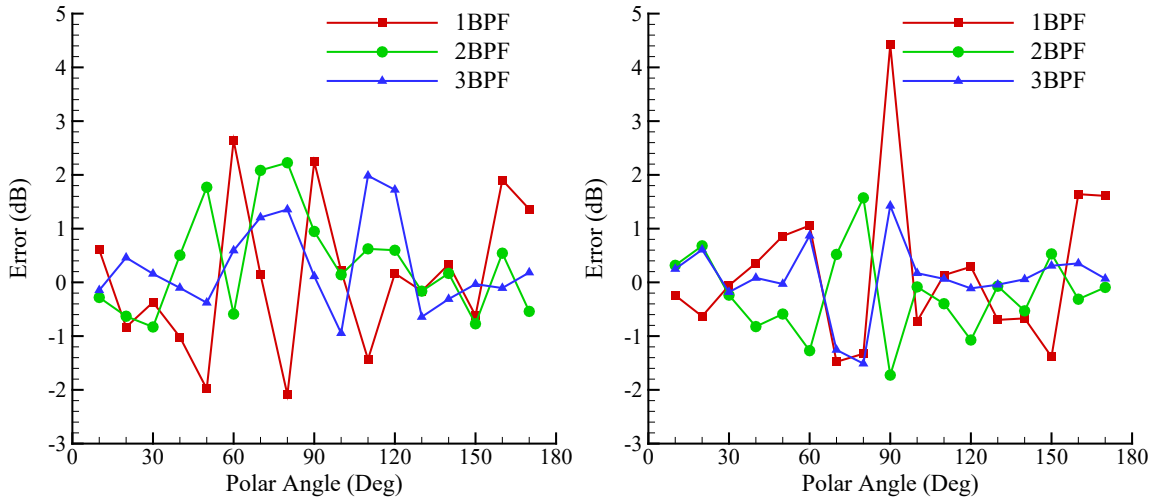

Fig. 15 Errors from treating inlet and aft tones as incoherent for flyover (left) and lateral (right) location.

Fig. 15 shows the errors of the second approach compared to the first for the case of two engines. The errors are defined as the incorrect approach minus the correct approach. The left plot is for the flyover locations under the flight path and the right plot is for lateral locations at 60 degrees in azimuthal angle from the flyover. In both plots, the first three BPF tones are shown. The results show that the incorrect approach can over- or under-predict by as much as 2 dB at flyover locations. At lateral locations, the over-prediction can be as much as 4 dB and the under-prediction, as much as 2 dB, which are significant in many ways, including for ground contours, for example. There are three types of interferences for tonal noise, namely, between propagation/scattering paths, between noise components, and between engines. The errors illustrated in Fig. 15 are from only the component interferences. If the tonal noise is treated completely as incoherent, the errors are more significant.

In addition to using the correct approach to calculate the scattering effects, it is also important to have the correct geometry model for the scattering. The details of the geometry very often control the dominant scattering features. Some examples have already been discussed in the previous sections, including the strong scattering of aft fan noise to forward angles by the local curved surfaces of the wings and the strong scattering to the lateral locations by the surfaces between the engines. It is common in aircraft system noise predictions that the scattering effects of the airframe are often treated in very rudimentary ways. In the WING module of ANOPP, for example, the aircraft geometry is simply represented by a flat plate and the scattering is accounted for by reflections of the flat plate and the diffractions by its sharp edges. As analyzed in the previous sections, the full configuration aircraft geometry plays an important role in the scattering patterns and amplitudes. To further demonstrate, a comparison study is performed, with a flat plate model extracted from the Boeing 787 aircraft by representing the wings and the fuselage by plates, as required by the WING module. The two geometry models are shown in Fig. 16, with the real aircraft geometry on the left and the flattened model on the right. This simplistic planar geometry model is used to calculate the scattering of engine fan noise by WING and the results are compared with those for the full configuration aircraft calculated by the much more capable PAASc method.

Fig. 16 Airframe geometry model of the Boeing 787 aircraft (left) and its flat plate simplification (right).

The scattering of broadband fan noise by the flat plate model is shown in Fig. 17, with the inlet component in the left plot and the aft fan component in the right plot, both for the 1000 Hz 1/3 octave band. This figure is intended for comparison with Fig. 10. The calculations for the two cases are identical, except for the geometry and the two scattering methods. The results in the two figures are plotted in the same formats, including the amplitude scales, for easy comparison. Clearly, WING with the flat plate geometry misses important scattering features in both the scattering patterns and amplitudes. In general, WING with the flat plate geometry significantly under-predicts the scattering effects.

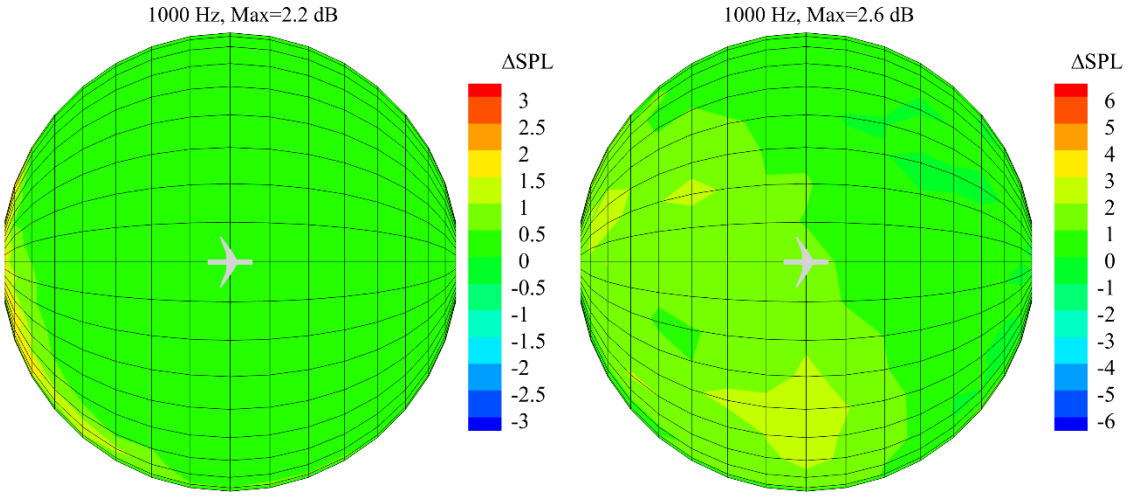

Fig. 17 Scattering of broadband fan noise by WING with the planar geometry, for inlet (left) and aft (right) components.

VII. Summary

A study has been presented for aircraft engine fan noise scattering by the airframe, using a new methodology and formulation implemented in a code designed for the requirements of aircraft system noise studies, the PAASc code. The methodology starts from the framework of geometric acoustics and adds significant extensions and improvements to account for features that are important for aircraft noise but are absent in classic geometric acoustics, including the presence of mean flows, the fully three dimensional noncanonical geometry, and the option for acoustic lining on the scattering surfaces. Another key to a practical scattering calculation, the method for engine fan noise source parameterization, has been presented and discussed, based on the method of least squares fitting with physical constraints. The method uses far field noise of isolated engines as inputs and derives important source features for scattering calculation, such as the source amplitude and directivity.

The important feature of source coherence has been discussed, and examples have been given to demonstrate its effects, both in experimental data and in computation. Coherent sources are characterized by constructive and destructive interferences, resulting in sharp peaks and dips in the resulting sound field, while radiation from an incoherent source is more gradually varying in both frequency and spatial domain. An example of experimental measurement has been presented for each source type, clearly demonstrating these features. Scattering calculations for both examples have been discussed and compared with data, showing very good agreements when the source features, coherent or incoherent, are correctly specified. The implementation of source coherence features in the scattering calculation is a unique capability in the methodology used in this paper.

The scattering results calculated for the Boeing 787 aircraft have been presented and analyzed, for both the inlet and the aft fan component, and for both the broadband and the tonal noise. It has been shown that many features are consistent with, and/or provide explanations for, observations in flight test data. These include the strong forward scattering of the aft fan noise, by the curved surfaces of the wing leading edge areas, to angles close to and upstream of the overhead position, and the strong scattering to the lateral locations, by the surfaces between the engines, both of which have been observed in aircraft flight tests. The forward scattering of aft fan noise, together with the flight effects of Doppler amplification and fan duct flow refraction, has been shown to move the peak radiation angle of the aft fan noise of isolated engines from the aft quadrant upstream to angles closer to the overhead angle.

The approach, formulation, and capabilities described in this study and contained in the PAASc code represents a significant improvement in aircraft scattering prediction methods compared to earlier rudimentary, over-simplified methods. The improvements are in accuracy of results and fidelity to the realism of aircraft geometry and operating conditions and these improvements have been validated with research quality, flight test data. It is important to note that PAASc meets the system noise requirements for fully 3D geometries with complex features and yet has extremely fast run times on the order of minutes for full scale aircraft, well within the range required for a versatile and effective design capability.

Acknowledgments

The support of the NASA Advanced Air Transport Technology Project is gratefully acknowledged, and the authors would like to thank the Boeing Company for allowing the use of the Boeing 787 aircraft geometry in the scattering calculations.

References

[1] Thomas, R.H., Burley, C.L., and Olson, E.D., "Hybrid Wing Body Aircraft System Noise Assessment with Propulsion Airframe Aeroacoustic Experiments," *International Journal of Aeroacoustics*, Vol. 11 (3+4), pp. 369-410, 2012. doi:10.1260/1475-472X.11.3-4.369

[2] Czech, M.J., Thomas, R.H., and Elkoby, R., "Propulsion Airframe Aeroacoustic Integration Effects of a Hybrid Wing Body Aircraft Configuration," *International Journal of Aeroacoustics*, Vol. 11 (3+4), pp. 335-368, 2012.

[3] Elkoby, R., "Full-Scale Propulsion Airframe Aeroacoustics Investigation," AIAA 2005-2807, 11th AIAA/CEAS Aeroacoustics Conference, Monterey, CA, May 2005.

[4] Czech, M.J. and Thomas, R.H., "Open Rotor Aeroacoustic Installation Effects for Conventional and Unconventional Airframes," AIAA Paper 2013-2185.

[5] Thomas, R.H., Burley, C.L., and Nickol, C.L., "Assessment of the Noise Reduction Potential of Advanced Subsonic Transport Concepts for NASA's Environmentally Responsible Aviation Project," AIAA Paper 2016-0863, 54th AIAA Aerospace Sciences Meeting, San Diego, California, January 4-8, 2016. doi:10.2514/6.2016-0863

[6] Thomas, R.H., Guo, Y., Berton, J.J., and Fernandez, H., "Aircraft Noise Reduction Technology Roadmap Toward Achieving the NASA 2035 Noise Goal," AIAA Paper 2017-3193, 23rd AIAA/CEAS Aeroacoustics Conference, Denver, Colorado, June 5-9, 2017. doi:10.2514/6.2017-3193

[7] Clark, I.A., Thomas, R.H., and Guo, Y., "Aircraft System Noise of the NASA D8 Subsonic Transport Concept," *AIAA Journal of Aircraft*, Vol. 58, No. 5 (2021), pp. 1106-1120. doi:10.2514/1.C036259

[8] June, J.C., Thomas, R.H., Guo, Y., and Clark, I.A., "Far Term Noise Reduction Technology Roadmap for a Large Twin-Aisle Tube-and-Wing Subsonic Transport," AIAA Paper 2019-2428, 25th AIAA/CEAS Aeroacoustics Conference, Delft, The Netherlands, May 20-23, 2019. doi:10.2514/6.2019-2428

[9] June, J.C., Thomas, R.H., and Guo, Y., "System Noise Reduction Roadmaps for both a Transonic Truss-Braced Wing and a Peer Conventional Configuration," AIAA Paper 2022-3049, 28th AIAA/CEAS Aeroacoustics Conference, Southampton, UK, June 14-17, 2022. doi:10.2514/6.2022-3049

[10] Czech, M., Thomas, R. H., Guo, Y., June, J. C., Clark I. A. and Shoemaker C., "Propulsion Airframe Aeroacoustics and Aircraft System Noise Flight Test on the Boeing 2020 ecoDemonstrator Program," AIAA 2022-2994, 28th AIAA/CEAS Aeroacoustics Conference, Southampton, UK, May 2022.

[11] Thomas, R. H., Guo, Y., Clark, I. A., June, J. C., "Propulsion Airframe Aeroacoustics and Aircraft System Noise Flight Research Test: NASA Overview," AIAA 2022-2993, 28th AIAA/CEAS Aeroacoustics Conference, Southampton, UK, May 2022.
[12] Preisser, J. S. and Chestnutt, D., "Flight Effects on Fan Noise with Static and Wind-Tunnel Comparisons," *J. Aircraft*, Vol. 21 No. 7, pp 453-461,1984.
[13] Clark, L., Thomas, R., Dougherty, R., Farassat, F. and Gerhold, C., "Inlet Shape Effects on the Far-Field Sound of a Model Fan," AIAA Paper 97-1589.
[14] Thomas, R.H., Farassat, F., Clark, L.R., Gerhold, C.H., Kelly, J.J., and Becker, L.E., "A Mode Detection Method Using the Azimuthal Directivity of a Turbofan Model," AIAA 99-1954, 5th AIAA/CEAS Aeroacoustics Conference, Bellevue, WA, May, 1999.
[15] Hubbard, H. (editor), "Aeroacoustics of Flight Vehicles: Theory and Practice, Volume 1: Noise Sources," NASA Reference Publication 1258, August,1991. URL:https://ntrs.nasa.gov/citations/19920001380
[16] Envia, E., "Fan Noise Reduction: An Overview," AIAA Paper 2001-0661, 39th Aerospace Sciences Meeting, Reno, NV, January 2001.
[17] Dahl. M. (editor), "Assessment of NASA's Aircraft Noise Prediction Capability," NASA TP 2012-215653, July 2012. URL:https://ntrs.nasa.gov/citations/20120012957
[18] Clark, I. A., Thomas, R. H. and Guo, Y., "Fan Acoustic Flight Effects on the PAA & ASN Flight Test," AIAA 2022-2996, 28th AIAA/CEAS Aeroacoustics Conference, Southampton, UK, May 2022.
[19] Guo, Y., Thomas, R.H., Clark, I.A., and June, J.C., "Far-Term Noise Reduction Roadmap for the Midfuselage Nacelle Subsonic Transport," *J. Aircraft*, Vol. 56, No. 5, pp. 1893-1906, 2019.
[20] Guo, Y., and Thomas, R.H., "System Noise Assessment of Hybrid Wing-Body Aircraft with Open-Rotor Propulsion," *J. Aircraft*, Vol. 52, No. 6, pp. 1767-1779, 2015.
[21] Clark, I. A., Nesbitt, E., Thomas, R. H. and Guo, Y., "Turbofan Aft-Radiated Broadband Acoustic Flight Effects," AIAA Paper 2024-3225, 30th AIAA/CEAS Aeroacoustics Conference, Rome, IT, June 2024.
[22] Nesbitt, E., Clark, I. A., Guo, Y., Thomas, R. H., "Flight Effects on Turbofan Fan Tones," AIAA Paper 2024-3222, 30th AIAA/CEAS Aeroacoustics Conference, Rome, IT, June 2024.
[23] Guo, Y., Pope, D.S., Burley, C.L., and Thomas, R.H., "Aircraft System Noise Shielding Prediction with a Kirchhoff Integral Method," AIAA Paper 2017-3196.
[24] Ganci, S., "A General Scalar Solution for the Half-plane Problem," J. Mod. Opt., 42(8):1707–1711, August 1995.
[25] Umul, Y. Z., "Young-Kirchhoff–Rubinowicz Theory of Diffraction in the Light of Sommerfeld's Solution," J. Opt. Soc. Am. A., 25(11):2734–2742, November 2008.
[26] Levy, B. and Keller, J. B., "Diffraction by a Smooth Object," *Communications on Pure and Applied Mathematics*, Vol. 12, 1959, pp. 159–209.
[27] Keller, J., "Rays, Waves and Asymptotics," Bulletin of the Am. Math. Soc. **84**(5), 727-750, 1978.
[28] Guo, Y. and Thomas, R. H., "Geometric Acoustics for Aircraft Noise Scattering," AIAA Paper 2022-3077, 28th AIAA/CEAS Aeroacoustics Conference, Southampton, UK, June 2022.
[29] Guo, Y., "Diffraction by Sharp Edges of Noncanonical Shape with Mean Flow and Surface Impedance," AIAA Paper 2024-3000, 30th AIAA/CEAS Aeroacoustics Conference, Rome, IT, June 2024.
[30] Thomas, R.H. and Guo, Y., "Systematic Validation of the PAAShA Shielding Prediction Method," *International Journal of Aeroacoustics*, Vol. 21(5-7), pp. 558-584, 2022.
[31] Thomas, R. H., Guo, Y., Nesbitt, E., Clark, I.A., and June, J.C., "Refined Predictions Compared with the Propulsion Airframe Aeroacoustics and Aircraft System Noise Flight Research Test Data," ICAS2024_0069, 34th Congress of the International Council of the Aeronautical Sciences (ICAS), Florence, IT, September 2024.
[32] Nesbitt, E.H., "Current Engine Noise and Reduction," *CEAS Aeronautical Journal*, Vol. 10, pp. 93 - 100, 2019.
[33] Hutcheson, F.V., Bahr, C.J., Thomas, R.H., and Stead, D.J., "Experimental Study of Noise Shielding by a NACA 0012 Airfoil," AIAA Paper 2018-2821, 24th AIAA/CEAS Aeroacoustics Conference, Atlanta, GA, May 2018.
[34] Hutcheson, F. V., Brooks, T. F., Burley, C. L., Bahr, C. J., Stead, D. J. and Pope, D. S. "Shielding of Turbomachinery Broadband Noise from a Hybrid Wing Body Aircraft Configuration," AIAA 2014-2624, 20th AIAA/CEAS Aeroacoustics Conference, Atlanta, GA, 2014.
[35] Beranek, L.L., *Noise and Vibration Control*, McGraw-Hill Book Company, 1971, pp. 174-180.
[36] Maekawa, Z., *Noise Reduction by Screens*, Applied Acoustics, Elsevier Publishing Co., Ltd., 1968, pp. 157-173.
[37] Krejsa, E.A. and Stone, J.R., "Enhanced Fan Noise Modeling for Turbofan Engines," NASA CR-2014-218421, December 2014. URL:https://ntrs.nasa.gov/citations/20150000884